A Domain Decomposition Method for the Vector Wave Equation

Bruno Stupfel and Martine Mognot

***Abstract*—A nonoverlapping domain decomposition method (DDM) is presented for the finite-element (FE) solution of electromagnetic scattering problems by inhomogeneous three-dimensional (3-D) bodies. The computational domain is partitioned into concentric subdomains on the interfaces of which conformal vector transmission conditions are prescribed and that can be implemented in the inhomogeneous part. The DDM is numerically implemented when a conformal vector absorbing boundary condition (ABC) is utilized on the outer boundary terminating the FE mesh, while employing the standard edge-based FE formulation. Then, numerical experiments are performed on a sphere and a cone sphere that emphasize the advantages of this technique in terms of memory storage and computing times, especially when the total number of unknowns is very large. Also, these numerical experiments serve as a severe test for the performances of the ABC.**

***Index Terms*—Electromagnetic scattering, finite-element method.**

I. Introduction

THE finite-element method (FEM) is a powerful numerical technique for solving scattering problems involving inhomogeneous arbitrarily shaped three-dimensional (3-D) objects. For open region problems, the radiation condition may be taken into account either rigorously by prescribing an integral equation (IE) on the surface of the object [1]–[4] or approximately by implementing on the outer boundary terminating the FE mesh an absorbing boundary condition (ABC) [5]–[10] or a perfectly matched absorber (PMA) [11]–[14]. When the size of the computational domain is electrically large, the number of unknowns may be such that all these techniques involve considerable computing times and memory storage requirements. Also, the generation of the FE mesh may constitute an insurmountable bottleneck. A possible way to circumvent these difficulties is to employ a domain decomposition method (DDM) that allows the decomposition of a large problem into several coupled subproblems that can be solved independently. A DDM specific to the solution of a scattering problem has been originally proposed in [15]–[18] where the subdomains are chosen to be the cubic cells of the FE mesh (see also [19]). In order to accelerate the convergence of the DDM iterative algorithm, this method has been adapted for the two-dimensional (2-D) case to a particular "onion-like" partition of the computational domain into concentric subdomains circumscribing the object (see Fig. 1), and conformal second-order scalar transmission conditions (TC's) and ABC's have been employed [20].

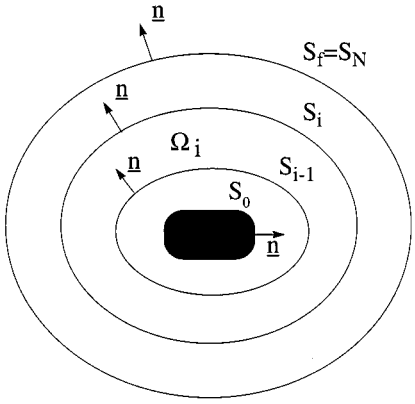

Fig. 1. "Onion-like" partition of the computational domain Ω.

In this paper, we present the extension of the abovementioned DDM to the solution of 3-D scattering problems when a conformal vector ABC [7] is applied on the terminating outer boundary. The corresponding conformal TC's can be implemented in the inhomogeneous domain instead of being applied in free-space exclusively, as was originally done in [20], thus authorizing the desired reduction in memory storage and mesh size. Also, it allows one to carry on the evaluation of the numerical performances of this ABC initiated in [10] since the boundary can be placed farther away from the surface of the scatterer. The organization of this paper is as follows. In Section II, we present the electromagnetic scattering problem to be solved and the DDM algorithm employed. In Section III the numerical implementation of the DDM is outlined for an edge-based FEM and the issue of its numerical complexity is addressed. Section IV is devoted to numerical experiments performed first on a sphere and then on a cone sphere with a high dynamic range for the radar cross section (RCS), which serves as a severe test for the performances of the DDM as well as of the ABC. Section V outlines conclusions and suggestions for future work.

II. Statement of the Problem and DDM Formulation

The problem to be solved is formulated in Section II-A and the DDM is presented in Section II-B.

A. Scattering Problem

A monochromatic incident wave ($\underline{E}^{\mathrm{inc}}$, $\underline{H}^{\mathrm{inc}}$) illuminates a penetrable inhomogeneous body immersed in free-space. $\underline{E}$ designates the electric field and $\underline{H}$ the magnetic field times

Manuscript received June 14, 1999; revised January 19, 2000.

The authors are with CEA/CESTA, Commissariat à l'Énergie Atomique, B.P. 2, 33114 Le Barp, France.

Publisher Item Identifier S 0018-926X(00)03256-7.

the free-space impedance η_0. $k_0 = 2\pi/\lambda_0$ is the wave number of the incident field and the assumed time dependence is $\exp(i\omega t)$. The Leontovich impedance boundary condition (LIBC) is prescribed upon the surface S_0 of the scatterer, which may be coated by inhomogeneous materials of relative dielectric permittivity ϵ and magnetic permeability μ that are position dependent 3×3 tensors. To alleviate the notations, the dependence of all quantities on the coordinates is suppressed throughout. In the infinite domain exterior to S_0, $\underline{H}$ satisfies the vector wave equation

$$\underline{\nabla} \times [\epsilon^{-1} \underline{\nabla} \times \underline{H}] - k_0^2 \mu \underline{H} = 0, \quad \underline{\nabla}.(\mu \underline{H}) = 0$$
$$\underline{E} = -\frac{i}{k_0} \epsilon^{-1} \underline{\nabla} \times \underline{H} \tag{1a}$$

and the LIBC on S_0

$$\underline{n} \times \epsilon^{-1} \underline{\nabla} \times \underline{H} = -ik_0 Z \underline{H}_{tg}. \tag{1b}$$

$\underline{n}$ designates the outward normal to S_0 as well as to all the surfaces that are considered in the following, Z is the normalized impedance assumed to be constant on S_0, and $\underline{H}_{tg} = -\underline{n} \times (\underline{n} \times \underline{H})$. $\underline{H} = \underline{H}^{\text{inc}} + \underline{H}^s$, $\underline{E} = \underline{E}^{\text{inc}} + \underline{E}^s$ and the second-order ABC in [7] (termed ABC2) is prescribed upon the outer boundary S_f terminating the computational domain Ω ($\partial\Omega = S_0 \cup S_f$) $-S_f$ must be convex and located in free-space

$$\underline{n} \times \underline{\nabla} \times \underline{H}^s = \underline{\underline{\beta}} \underline{H}^s_{tg} + \gamma (L_R + L_D) \underline{H}^s_{tg}. \tag{1c}$$

For an arbitrary vector $\underline{V}$ tangent to S_f, the tangential operators L_R and L_D are defined as

$$L_R(\underline{V}) = \underline{\nabla} \times \{\underline{n} (\underline{\nabla} \times \underline{V})_n\}, \quad L_D(\underline{V}) = \underline{\nabla}_{tg} (\underline{\nabla}.\underline{V}_{tg}).$$

The subscript n denotes the scalar product with $\underline{n}$ and

$$\underline{\underline{\beta}} \underline{t}_1 = [-2k^2 + (3\kappa_2 + \kappa_1)(ik + (\kappa_2 - \kappa_1)/4)\, \underline{t}_1] \cdot /[2(ik + 2\kappa_m)]$$
$$\underline{\underline{\beta}} \underline{t}_2 = [-2k^2 + (3\kappa_1 + \kappa_2)(ik + (\kappa_1 - \kappa_2)/4)\, \underline{t}_2] \cdot /[2(ik + 2\kappa_m)]$$
$$\gamma = (1 - i\kappa_m/k)/[2(ik + 2\kappa_m)].$$

The orthonormal vectors $\underline{t}_1$, $\underline{t}_2$ are tangent to S_f along the principal lines of curvature ($\underline{n} = \underline{t}_1 \times \underline{t}_2$), κ_1, κ_2 are the principal curvatures of S_f counted positively where S_f is convex, and $\kappa_m = (\kappa_1 + \kappa_2)/2$. For the zeroth-order ABC (termed ABC0), we have

$$\underline{\underline{\beta}} = ik_0 (\underline{t}_1 \underline{t}_1 + \underline{t}_2 \underline{t}_2), \quad \gamma = 0.$$

The problem to be solved, as constituted by equations (1a)–(1c), is termed P_{ABC}.

B. DDM Algorithm

Now we formulate the DDM algorithm. Ω contains the inhomogeneous medium and is partitioned into N concentric subdomains Ω_i, $1 \le i \le N$. S_{i-1} and S_i denote, respectively, the inner and outer boundaries of Ω_i, and $S_f = S_N$ (see Fig. 1). The algorithm defined in [20] for a 2-D problem is extended to

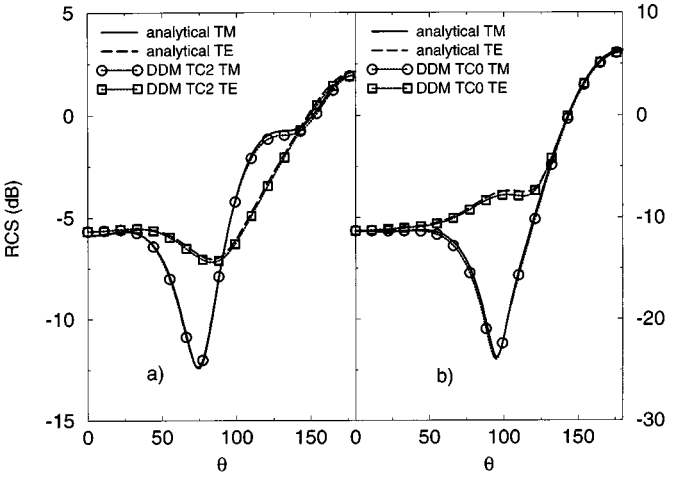

Fig. 2. PEC sphere (500 MHz): Bistatic RCS computed with an ABC2 on S_f from the closed-form solution and the DDM solution with $N = 3$. (a) $\epsilon = \mu = 1$ everywhere and TC2. (b) $\epsilon = 1 - i$, $\mu = (1 - i)/2$ in Ω_1 and TC0.

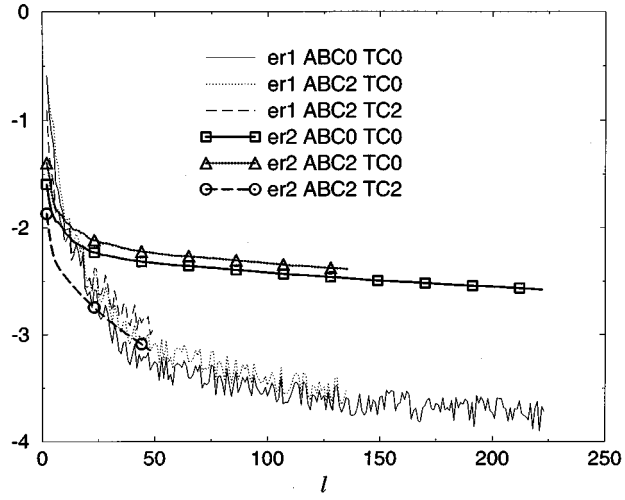

Fig. 3. PEC sphere (500 MHz); $er1$, $er2$ versus ℓ. $N = 3$, $\epsilon = \mu = 1$ everywhere and $\epsilon_{\text{CG}} = 10^{-6}$.

a 3-D problem as follows . Let $\underline{E}_i^\ell$, $\underline{H}_i^\ell$ be the values of the fields in Ω_i at iteration ℓ. They satify Maxwell's equations in Ω_i

$$\underline{\nabla} \times [\epsilon^{-1} \underline{\nabla} \times \underline{H}_i^\ell] - k_0^2 \mu \underline{H}_i^\ell = 0$$
$$\underline{\nabla}.(\mu \underline{H}_i^\ell) = 0$$
$$\underline{E}_i^\ell = -\frac{i}{k_0} \epsilon^{-1} \underline{\nabla} \times \underline{H}_i^\ell \tag{2a}$$

and the following TC's on $\partial\Omega_i = S_{i-1} \cup S_i$:

$$T^- \underline{H}_i^\ell = T^- \underline{H}_{i-1}^\ell \quad TC\ on\ S_{i-1}$$
$$T^+ \underline{H}_i^\ell = T^+ [\alpha_\ell \underline{H}_i^{\ell-1} + (1 - \alpha_\ell) \underline{H}_{i+1}^{\ell-1}] \quad TC\ on\ S_i \tag{2b}$$

with

$$T^\pm \underline{H} = \pm \underline{n} \times [\epsilon^{-1} \underline{\nabla} \times \underline{H}] - \left[\underline{\underline{\beta}} + \gamma (L_R + L_D)\right] \underline{H}_{tg}. \tag{2c}$$

The values of $\underline{\underline{\beta}}$, γ are those computed on S_{i-1}, S_i, and α_ℓ is the relaxation parameter that accelerates the convergence of the algorithm: $\alpha_1 = 0$ and $0 \le \alpha_\ell \le 1/2$, $\ell \ge 2$. To alleviate

the notations, it is understood that the values of ϵ implicitly involved in (2b) are those corresponding to the electric field [see definition (2c) of $T^{\pm}$]: Considering, e.g., the first TC in (2b), the values of ϵ in the left-hand side (LHS) are those on S_{i-1} coming from Ω_i, while the values of ϵ in the right-hand side (RHS) are those on S_{i-1} coming from Ω_{i-1}, and ϵ may be discontinuous on the interfaces. For $i = 1$, the LIBC (2.1b) is substituted to the TC on S_0

$$\underline{n} \times \epsilon^{-1} \underline{\nabla} \times \underline{H}_1^{\ell} = -ik_0 Z \underline{H}_{1tg}^{\ell}. \tag{2d}$$

For $i = N$, the ABC (1c) is substituted to the TC on S_N

$$T^{+} \underline{H}_N^{\ell} = T^{+} \underline{H}^{\text{inc}}. \tag{2e}$$

The initial values are chosen to be

$$\underline{H}_i^{\ell=0} = \underline{H}^{\text{inc}} \qquad 1 \le i \le N. \tag{3}$$

For each value of ℓ, the problems P_i^{ℓ} corresponding to equations (2a)–(2e) are solved successively for increasing values of i, $1 \le i \le N$. On account of (3), the solution of P_1^1 is identical to the one of P_{ABC} with $S_f = S_1$. Increasing i amounts to propagate the scattered field up to the terminating boundary S_f through the first TC in (2b). Thus ($\underline{E}^1$, $\underline{H}^1$) may be considered as an initial value for the iteration $\ell = 2$. For $\ell \ge 2$, the algorithm propagates similarly the scattered field through the successive subdomains up to S_f. It also takes into account, through the second TC in (2b), the scattered field, calculated at the previous iteration, which results from the spurious reflections on the successive interfaces and on S_f where approximate TC's and radiation condition are prescribed, respectively. It is important to note that when the ABC and TC's are of zeroth-order and ϵ, μ are diagonal and correspond to passive materials, it has been demonstrated in [21] that the solutions of this algorithm tend to those of problem P_{ABC} as ℓ goes to infinity, independently of the choice made for the initial values.

III. Numerical Implementation

For problem P_i^{ℓ}, the variational formulation equivalent to the wave equation in (2a) is, after integrating by parts

$$\int_{\Omega_i} \left\{ (\underline{\nabla} \times \underline{\tilde{H}}) . \epsilon^{-1} (\underline{\nabla} \times \underline{H}_i^{\ell}) - k_0^2 \underline{\tilde{H}} . \mu \underline{H}_i^{\ell} \right\} d\Omega - \int_{S_{i-1}} \underline{\tilde{H}} . (\underline{n} \times [\epsilon^{-1} \underline{\nabla} \times \underline{H}_i^{\ell}]) \, dS + \int_{S_i} \underline{\tilde{H}} . (\underline{n} \times [\epsilon^{-1} \underline{\nabla} \times \underline{H}_i^{\ell}]) \, dS = 0.$$

$\underline{\tilde{H}}$ is a test function. Because of the definition (2c) of the $T^{\pm}$ operator, we have

$$\int_{\Omega_i} \left\{ (\underline{\nabla} \times \underline{\tilde{H}}) . \epsilon^{-1} (\underline{\nabla} \times \underline{H}_i^{\ell}) - k_0^2 \underline{\tilde{H}} . \mu \underline{H}_i^{\ell} \right\} d\Omega + \int_{S_{i-1}} \underline{\tilde{H}}_{tg} . \left[\underline{\underline{\beta}} + \gamma (L_R + L_D) \right] \underline{H}_{itg}^{\ell} \, dS + \int_{S_i} \underline{\tilde{H}}_{tg} . \left[\underline{\underline{\beta}} + \gamma (L_R + L_D) \right] \underline{H}_{itg}^{\ell} \, dS = b_i^{\ell} \tag{4a}$$

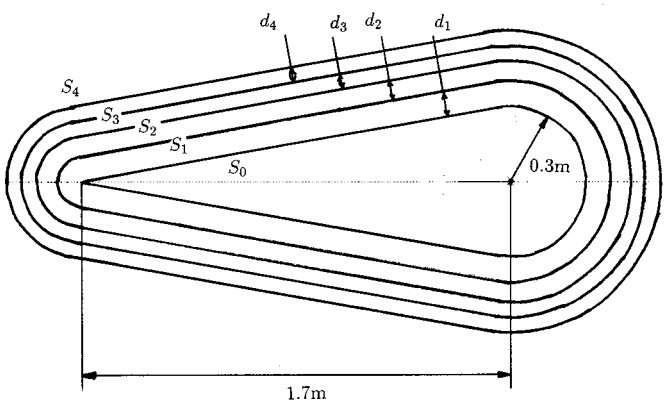

Fig. 4. Geometry of the cone sphere and partition of the computational domain.

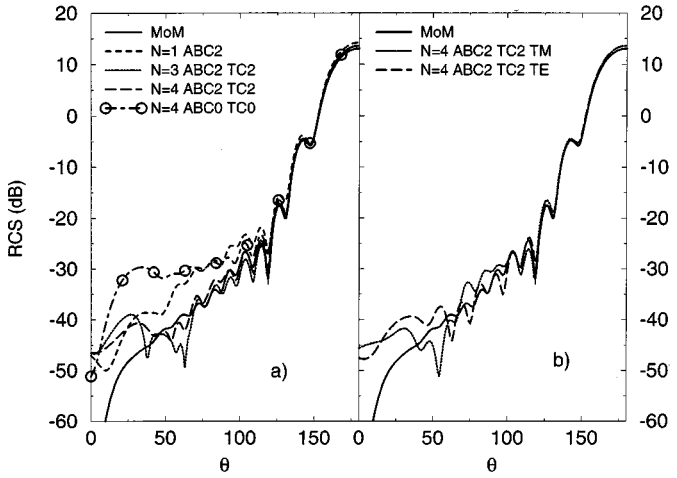

Fig. 5. Cone sphere with $Z = 1$ and $\epsilon = \mu = 1$ everywhere. 800 MHz and $\theta^{\text{inc}} = 0$. (a) Mean RCS for $N = 1, 3, 4$, ABC2, TC2 and $N = 4$, ABC0, TC0. (b) RCS for $N = 4$, ABC2 and TC2.

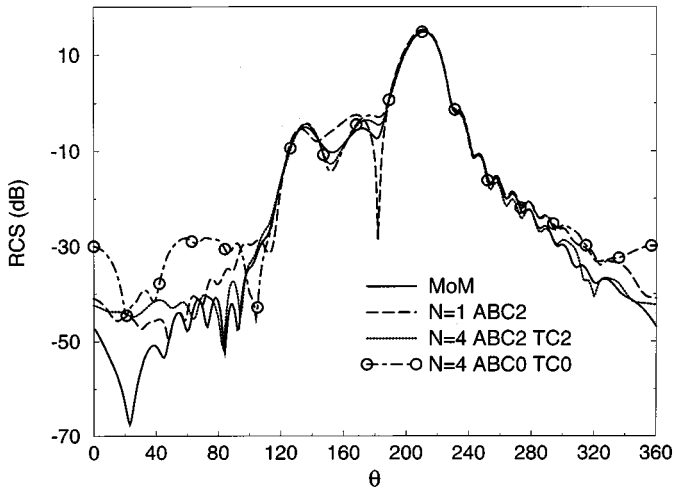

Fig. 6. Same as Fig. 5. $\theta^{\text{inc}} = 30°$. Mean RCS.

with

$$b_i^{\ell} = -\int_{S_{i-1}} \underline{\tilde{H}}_{tg} . T^{-} \underline{H}_i^{\ell} \, dS - \int_{S_i} \underline{\tilde{H}}_{tg} . T^{+} \underline{H}_i^{\ell} \, dS. \tag{4b}$$

When $i = 1$, the integral on S_0 in the LHS of (4a) is replaced by $ik_0Z \int_{S_0} \underline{\tilde{H}}_{tg}.\underline{H}^{\ell}_{1tg}\, dS$, and the one in the RHS of (4b) is zero. Similarly to what has been done in [20] it can be shown, by using the boundary conditions (2b), (2d) and (2e), that b_i^{ℓ} can be recursively calculated as follows:

• $i = 1$:

$$b_1^1 = -\int_{S_1} \underline{\tilde{H}}_{tg}.T^{+}\,\underline{H}^{\text{inc}}\, dS$$

$\ell \geq 2$:

$$b_1^{\ell} = b_1^{\ell-1} + 2(1-\alpha_{\ell}) \int_{S_1} \underline{\tilde{H}}_{tg}.\left[\underline{\underline{\beta}} + \gamma(L_R + L_D)\right] \cdot (\underline{H}^{\ell-1}_{2tg} - \underline{H}^{\ell-1}_{1tg})\, dS \tag{5a}$$

• $2 \leq i \leq N$:

$$\begin{aligned} b_i^1 = &-\int_{S_i} \underline{\tilde{H}}_{tg}.T^{+}\underline{H}^{\text{inc}}\, dS \\ &+ \int_{S_{i-1}} \underline{\tilde{H}}_{tg}.T^{+}\underline{H}^{\text{inc}}\, dS \\ &+ 2\int_{S_{i-1}} \underline{\tilde{H}}_{tg}.\left[\underline{\underline{\beta}} + \gamma(L_R + L_D)\right] \underline{H}^1_{(i-1)tg}\, dS \end{aligned}$$

$\ell \geq 2$:

$$\begin{aligned} b_i^{\ell} = &\, b_i^{\ell-1} + 2(1-\alpha_{\ell}) \int_{S_i} \underline{\tilde{H}}_{tg} \\ &\cdot \left[\underline{\underline{\beta}} + \gamma(L_R + L_D)\right] (\underline{H}^{\ell-1}_{(i+1)tg} - \underline{H}^{\ell-1}_{itg})\, dS \\ &+ 2\int_{S_{i-1}} \underline{\tilde{H}}_{tg}.\left[\underline{\underline{\beta}} + \gamma(L_R + L_D)\right] \\ &\cdot [\underline{H}^{\ell}_{(i-1)tg} - \underline{H}^{\ell-1}_{itg} + \alpha_{\ell}(\underline{H}^{\ell-1}_{itg} - \underline{H}^{\ell-1}_{(i-1)tg})]\, dS \end{aligned} \tag{5b}$$

with the convention that the integral on S_i in (5b) is zero when $i = N$ and $\ell \geq 2$. Then, the surface integrals in the LHS of (4a) and those in the RHS of (5a), (5b) are integrated by parts by virtue of the identities

$$\int_S \gamma \underline{\tilde{H}}.L_R(\underline{H}_{tg})\, dS = \int_S \gamma(\underline{\nabla} \times \underline{\tilde{H}})_n(\underline{\nabla} \times \underline{H})_n dS \tag{6a}$$

$$\int_S \gamma \underline{\tilde{H}}.L_D(\underline{H}_{tg}) dS = -\int_S \gamma(\underline{\nabla}.\underline{\tilde{H}}_{tg})\,(\underline{\nabla}.\underline{H}_{tg})\, dS \tag{6b}$$

obtained by dropping the terms involving the tangential derivatives of the curvatures, that have been any how neglected in the expression (1c) of the second-order ABC [7]. As in [10], each subdomain Ω_i is meshed with tetrahedrons, first-order edge-basis functions are employed and a Galerkin procedure is used. For second-order ABC and/or TC's, the discretization of the surface divergence terms in (4a), (5a), (5b) generated by the L_D operator [see (6b)] is performed as mentioned in [10]. The variational formulation (4a) is thus transformed into the following linear system

$$A_i H_i^{\ell} = b_i^{\ell} \tag{7}$$

where the matrix A_i is symmetric. Each subdomain is separately meshed and, in order to simplify the numerical implementation, the surface mesh of S_i generated by the volume meshing of Ω_{i+1} is chosen to be identical to the one of the same interface generated by the meshing of Ω_i. For each polarization TM or TE of the incident wave, and for fixed values of ℓ and i, we proceed as follows: 1) compute A_i; 2) read on binary files the previously computed quantities that are necessary for the calculation of b_i^{ℓ} and compute b_i^{ℓ}; and 3) solve system (7) with the same conjugate gradient (CG) than the one employed in [10] (the initial solution is $H_i^{\ell-1}$ and A_i is preconditioned by the diagonal); the CG is stopped when

$$||A_i H_i^{\ell} - b_i^{\ell}|| \leq \epsilon_{\text{CG}} \tag{8}$$

(here and in the following the L^2 norm is used); write on binary files the computed quantities that are used in the following steps. The algorithm is stopped when

$$||H_1^{\ell} - H_1^{\ell-1}|| \leq \epsilon_{\text{DDM}} \tag{9}$$

(ϵ_{CG}, ϵ_{DDM} control the accuracy of the results) and the RCS is computed from the values of $\underline{n} \times \underline{H}_1^{\ell}$ on S_0 if S_0 surrounded by free-space or else from those of $\underline{n} \times \underline{H}_i^{\ell}$, $\underline{n} \times \underline{E}_i^{\ell}$, $i < N$, on the interface S_i in contact with free-space (see Appendix).

If N_i^{el} of designates the number of elements in Ω_i, then the memory storage required for the solution of the whole problem is $O(\max_{i=1,\,N} N_i^{el})$ [10]. In other words, if the subdomains are constructed in such a way that they contain an identical number of elements, then the DDM divides by a factor approximately equal to N the memory size required for the solution of the entire problem P_{ABC}. Let N_i^{un} be the number of unknowns in Ω_i, n_i^{ℓ} the number of CG iterations required for the solution of problem P_i^{ℓ} and L the number of DDM iterations satisfying (9). Then, the total computing time is

$$\text{TCPU(DDM)} = O\left[\sum_{\ell=1}^{L}\sum_{i=1}^{N} n_i^{\ell}(N_i^{un})^2\right] \tag{10}$$

If N_i^{el} is the same for all subdomains, then $N_i^{un} \simeq N^{un}/N$ where N^{un} is the total number of unknowns for P_{ABC}. The numerical calculations performed in Section IV show that, for given orders of the ABC and TC's, n_i^{ℓ}/N_i^{un} can be bounded by a constant χ independent of ℓ and i (χ decreases when ℓ increases since the previous solution is used as an initial value for each CG). This implies $n_i^{\ell} < \chi N^{un}/N$ and (10) becomes

$$\text{TCPU(DDM)} < O\left[L\chi\frac{(N^{un})^3}{N^2}\right] \simeq \frac{L}{N^2}\ \text{TCPU}(P_{\text{ABC}}). \tag{11}$$

We note that the DDM is less costly, in terms of CPU times, than the solution of the entire problem P_{ABC} if $L < N^2$.

IV. Numerical Experiments

As in [10], all the numerical results presented in this section have been performed on bodies of revolution (BOR's): sphere and cone sphere. The boundary S_f and the interfaces are axisymmetric. No symmetry is taken into account. The meshes have been realized with IDEAS and are such that the length of most of the edges is smaller than $\lambda/10$. MoM or hybrid FE-IE codes for BOR's [22], [2] serve as references, and the calculations are performed on one processor of a Cray T90. In the examples presented here, only the first subdomain may contain materials and ϵ and μ are scalar. The value of the relaxation parameter α_{ℓ} as defined in Section II-B, is randomly chosen at each iteration. $\epsilon_{\text{DDM}} = 3\epsilon_{\text{CG}}$ [see (9)]—obviously, the accuracy required for the DDM algorithm must be lower than the one for the CG—and, unless otherwise mentioned, $\epsilon_{\text{CG}} = 10^{-2}$ [see

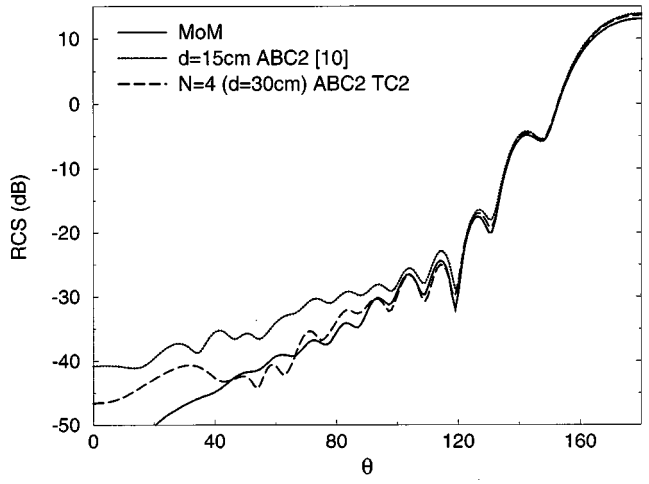

Fig. 7. Same as Fig. 5. $\theta^{\rm inc} = 0$. Mean RCS for $d = 15$ cm [10] and $d = 30$ cm (DDM).

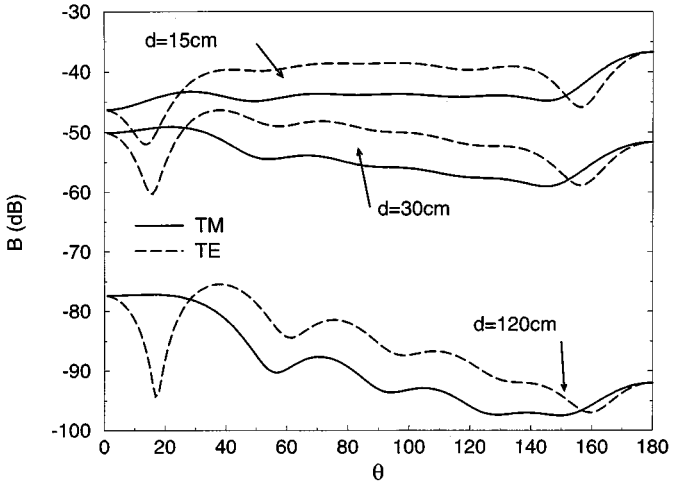

Fig. 8. $B(d, \theta)$ for the sphere $R = 30$ cm, ABC2 on S_f, 800 MHz.

(8)]: It has been found that these values have always ensured the RCS convergence. A complete calculation is necessary for each polarization and incidence angle, and the major part of the computing time is devoted to the solution of systems (7). Validation tests performed on a sphere are presented in Section IV-A, and Section IV-B is devoted to the cone sphere results.

A. Numerical Results for the Sphere

The radius of the perfectly conducting (PEC) sphere is 25 cm. $N = 3$ and the subdomains are spherical shells. The radii of S_1, S_2 and $S_3 = S_f$ are 30, 34 and 37 cm, respectively, so that the distance between S_0 and S_f is 12 cm. The calculation frequency is 500 MHz. First, $\epsilon = \mu = 1$ everywhere. We observe on Fig. 2(a) (bistatic RCS versus observation angle θ) a good agreement between the DDM results obtained in five iterations with second-order ABC and TC's (ABC2 and TC2) and those obtained in closed form for the $P_{\rm ABC}$ problem with an ABC2 on S_f [10]. The polarization conventions are as in [10]: TM (TE) corresponds to the incident magnetic (respectively electric) field transverse to the plane of incidence defined by the BOR's revolution axis and the direction of incidence. We get the same agreement with various values for the order of the ABC, the TC, the frequency, and N. For example, we have plotted on Fig. 2(b) the bistatic RCS obtained with the material $\epsilon = 1 - i$, $\mu = (1 - i)/2$ in Ω_1, an ABC2 on S_f and, for the DDM, a zero-order TC (TC0) on S_1 and S_2. Fig. 3 plots two types of error versus ℓ, viz. $er1$ and $er2$,

$$er1(\ell) = \log(\|H_1^\ell - H_1^{\ell-1}\|),$$
$$er2(\ell) = \log[\|H_{tgN}^\ell(S_{N-1}) - H_{tgN-1}^\ell(S_{N-1})\|]$$

obtained for $N = 3$, $\epsilon = \mu = 1$ everywhere, $\epsilon_{\rm CG} = 10^{-6}$ and various orders for the ABC and TC. In view of these results, we can readily draw the following conclusions.

The convergence of $er1(\ell)$ is approximately independent of the order of the ABC and TC, although slightly faster with the TC2 for low values of ℓ.

As it has been already observed in [20], $er2(\ell)$ decreases more rapidly with a TC2, thus demonstrating its superior efficiency.

TABLE I
CONE SPHERE:
NUMBER OF ELEMENTS N_i^{el} AND UNKOWNS N_i^{un} FOR EACH SUBDOMAIN Ω_i

	Ω_1	Ω_2	Ω_3	Ω_4
800MHz	$N_1^{el} = 75358$	$N_2^{el} = 89556$	$N_3^{el} = 83544$	$N_4^{el} = 105799$
	$N_1^{un} = 98534$	$N_2^{un} = 120355$	$N_3^{un} = 117917$	$N_4^{un} = 148383$
1.2GHz	$N_1^{el} = 284154$	$N_2^{el} = 332385$	$N_3^{el} = 320588$	$N_4^{el} = 386662$
	$N_1^{un} = 356245$	$N_2^{un} = 424269$	$N_3^{un} = 420779$	$N_4^{un} = 507678$

One may explain the different behaviors of $er1(\ell)$ and $er2(\ell)$ by the fact that the solution converges more rapidly on the periphery of the domain. For example, it can easily be shown from (5a), (5b) that the solution in Ω_1 is affected by the radiation condition on S_f only if $\ell \geq N$—this is the reason why the number of iterations increases with N—; hence, the stopping criterion (9) performed on the solutions in Ω_1 ensures the convergence of the solutions in each subdomain, but we may think that it is more advantageous to compute the RCS from the values of the fields on S_N, as it has been done in [20].

Since all the results have been obtained with the same computing times, we note that a calculation performed with an ABC2 and TC2 is roughly three times longer than a computation performed with an ABC2 and TC0, the reason for this being that the convergence of the CG for the solution of problem P_i^ℓ is all the slower as the order of the boundary conditions is high [10]. As a consequence, it is recommended to employ the TC0.

Finally, we have verified that the restart procedure defined in [20] for 2-D problems works also for 3-D problems: A first, computation performed with $N = 2$, followed by a restart where the last subdomain is added, yields identical results to those directly obtained with $N = 3$.

B. Numerical Results for the Cone Sphere

The cone sphere is identical to the one defined in [10]: the total length of the object is 2 m, the radius of the sphere 30 cm, and the tangent is continuous at the junction between the

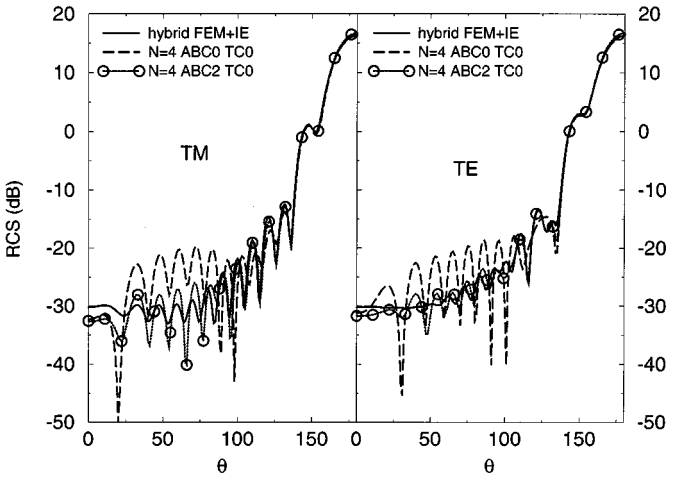

Fig. 9. PEC cone sphere coated with the material $\epsilon = 1 - i, \mu = (1 - i)/2$ in Ω_1; 800 MHz and $\theta^{\rm inc} = 0$.

sphere and the cone (see Fig. 4). Let us first mention that the various numerical experiments performed with this geometry show that the DDM behaves as indicated in Section IV-A. $N = 4$, the interfaces are conform to S_0, and the subdomains are such that they contain approximately the same number of elements. The values of the distances d_i separating the interfaces are, for increasing values of i, 10, 8, 6, and 6 cm, so that S_f is placed 30 cm away from S_0 (see Fig. 4). For all the examples presented below, only the bistatic RCS is computed.

The firsts results have been obtained at 800 MHz with $Z = 1$ and $\epsilon = \mu = 1$ everywhere: The overall length of the object is $5.44\,\lambda$ and the radius of the sphere $0.8\,\lambda$. The number of elements N_i^{el} and unknowns N_i^{un} in each subdomain Ω_i is given in Table I, with a total number of $\sum_{i=1}^{4} N_i^{un} = 485\,189$ unknowns. The number of elements and unknowns for the equivalent problem $P_{\rm ABC}$ solved without the DDM would have been 354 257 and 431 372, respectively (one must deduct the unknowns on the interfaces S_1 to S_3 that are shared by the contiguous subdomains). Fig. 5(a) plots the arithmetical mean of the RCS calculated for the two polarizations, i.e., (RCS(TM)+RCS(TE))/2, in axial incidence on the cone-tip ($\theta^{\rm inc} = 0$) for $N = 1, 3, 4$, with ABC2 and TC2 (as a comparison, we have plotted the results obtained with $N = 4$, ABC0 and TC0 and we recall that the exact RCS is polarization independent when $Z = 1$). This allows us to verify that the accuracy increases when S_f is placed farther away from the object—even if the arithmetical mean improves the results [see Fig. 5(b)]—independently of the angle of incidence (see Fig. 6: mean RCS for $\theta^{\rm inc} = 30°$). Fig. 7 compares the mean RCS calculated in [10] for axial, on tip incidence without the DDM for a distance $d = 15$ cm between S_0 and S_f with the one calculated with the DDM and $d = 30$ cm ($N = 4$). We observe that doubling the value of d allows us to obtain (for the mean RCS) an error smaller than 5 dB for RCS levels higher than -45 dB, instead of -30 dB for $d = 15$ cm. Actually the RCS error decreases more slowly from some value of d [cf. [10] and Fig. 5(a)]. If we compare the computational domain to an anechoid chamber, we can calculate analytically the numerical noise corresponding to a sphere of radius R with $Z = 1$ centered in a spherical domain on whose boundary, of radius $R + d$, is prescribed an ABC. If $F(d, \theta)$ denotes the far scattered field amplitude, then we may define the numerical noise $B(d, \theta)$ in dB as

$$B(d, \theta) = 10 \log[4\pi |F_{\rm ABC}(d, \theta) - F_{ex}(d, \theta)|^2] \qquad (12)$$

F_{ex} ($F_{\rm ABC}$) designates the exact (respectively computed with an ABC) amplitude. For a sphere of radius 30 cm (equal to the one of the spherical part of the cone sphere) and an ABC2, we get at 800 MHz the curves of Fig. 8 for $d = 15$, 30 and 120 cm: when d increases from 15–30 cm, the noise is effectively reduced by about ten dB, but a distance of 120 cm is necessary to get below -75 dB. On account of the fact that the forward scattering RCS ($\theta = 180°$) is 5 dB lower for the sphere than for the cone sphere, we may extrapolate that a good accuracy on RCS levels higher than -70 dB would be achieved for the cone sphere with d equal to about 1 m, while keeping in mind that the numerical noise for a given ABC depends on the shape of the object and on the impedance boundary condition (for a PEC, the noise is about ten decibels larger when the ABC2 is employed) on the incidence angle and on the shape of the "chamber." Indeed, we note that in view of Fig. 6 ($\theta^{\rm inc} = 30°$), that if the mean RCS is correctly computed with an ABC2 and $N = 4$ for levels that are higher than -40 dB, there is obviously a problem around 160°, although the RCS value is relatively large (about -10 dB). A calculation performed with $Z = 0$ at the same frequency, with the same subdomains and meshes, but with the material $\epsilon = 1 - i, \mu = (1 - i)/2$ substituted to free-space in Ω_1, yields a similar accuracy (ABC2 and $N = 4$: see Fig. 9) although the surface object S_1 is closer to the boundary S_4 ($d = 20$ cm). Again, one verifies the superior performances of the ABC2 over the ABC0.

Then, keeping the same subdomains, the average edges length of the FE cells has been reduced by 50% in order to perform calculations at 1.2 GHz. Now, the overall length of the object is $8.16\ \lambda$, the radius of the sphere $1.2\ \lambda$, and the corresponding values of N_i^{el} and N_i^{un} are given in Table I, with a total number of $\sum_{i=1}^{4} N_i^{un} = 1\,708\,971$ unknowns. The number of elements and unknowns for the equivalent problem $P_{\rm ABC}$ solved without the DDM would have been 1 323 789 and 1 604 233, respectively, involving considerable difficulties in the mesh generation and very large computer resources. The RCS has been computed for $\theta^{\rm inc} = 0°$ with $N = 4$, ABC2 and TC0, $Z = 1$ and $\epsilon = \mu = 1$ everywhere on one hand [Fig. 10a)], and $Z = 0$ on S_0, $\epsilon = 1$ and $\mu = (1 - i)/2$ in Ω_1 on the other hand [Fig. 10(b)]. The accuracy achieved is approximately the same than at 800 MHz [see Figs. 5(b) and 9] which confirms that, for a sufficiently high value of the frequency, the efficiency of an ABC depends on the distance d between the boundary and the surface of the object, rather than on d/λ [10]. Fig. 11 plots $B(d = 30\,\text{cm}, \theta)$ calculated at 1.2 GHz and 5 GHz for the sphere of radius 30 cm with $Z = 1$ and an ABC2 or the high-order ABC (HOABC) proposed in [10]. Again, it confirms that the ABC2's performances remain virtually unchanged at 5 GHz (except for the small values of θ) and that even the HOABC does not allow a noise reduction below -60 dB. These results

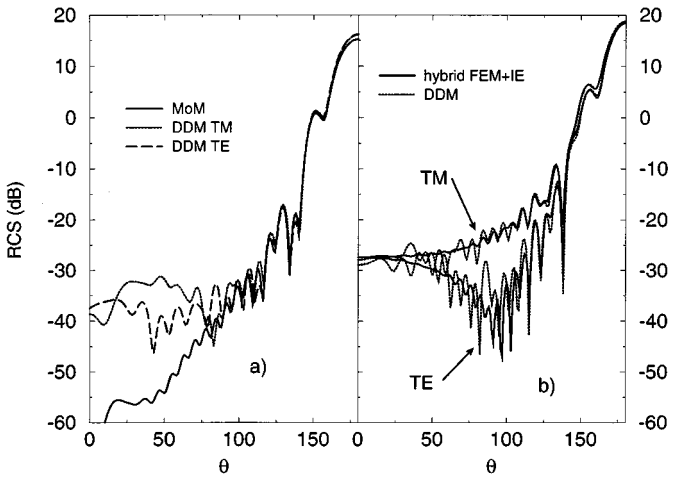

Fig. 10. Cone sphere: 1.2 GHz and $\theta^{\rm inc} = 0$. DDM with $N = 4$, ABC2 and CT0. (a) $Z = 1$ and $\epsilon = \mu = 1$ everywhere. (b) $Z = 0$ and $\epsilon = 1$, $\mu = (1 - i)/2$ in Ω_1.

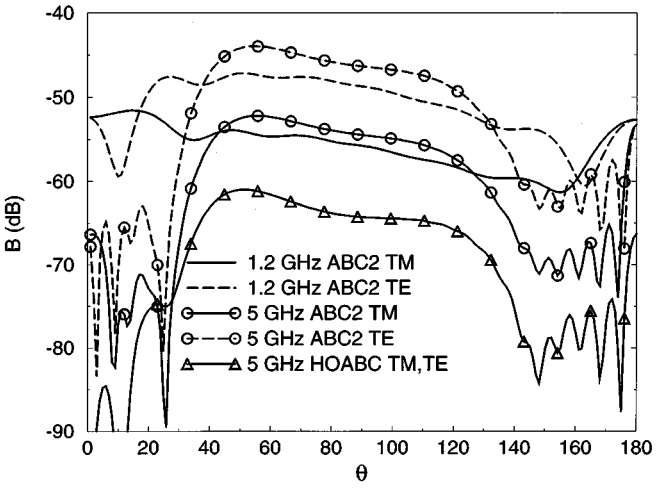

Fig. 11. $B(d = 30$ cm, $\theta)$ for the sphere $R = 30$ cm, ABC2 on S_f.

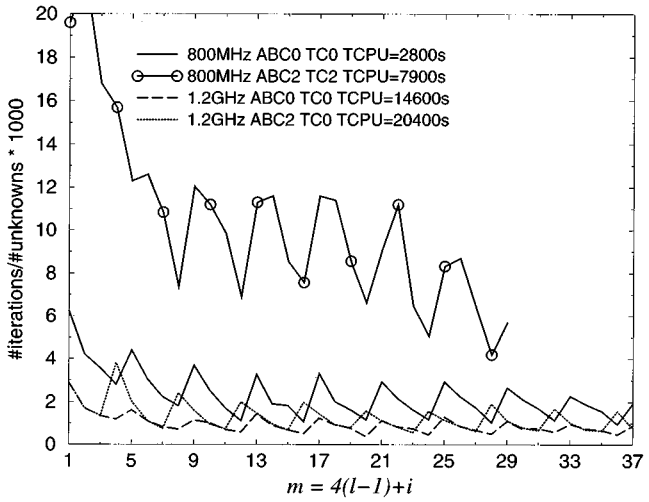

Fig. 12. Cone sphere: $10^3 n_i^\ell / N_i^{un}$ versus m with four subdomains.

are given as indications only, and one must be aware that their generalization to other geometries is not always justified.

On Fig. 12 is displayed $10^3 n_i^\ell / N_i^{un}$, i.e., the ratio of the number of CG iterations required for the solution of problem P_i^ℓ to the number of unknowns in Ω_i, multiplied by 10^3 versus $m = N(\ell - 1) + i$ for $N = 4$ $(1 \le i \le 4)$, $Z = 1$ and various ABC's and TC's at 800 MHz and 1.2 GHz. m represents the number of problems $P_{i'}^{\ell'}$ ($\ell' \le \ell$ and $i' \le i$) that have been solved during the iteration process. These plots show that the convergence of the CG is all the slower as the order of the boundary conditions for problem P_i^ℓ is high (as it has been already mentioned for the sphere in Section IV-A) and that, for a TC0, n_i^ℓ / N_i^{un} is almost independent of N_i^{un} and even lower for a three times denser mesh (1.2 GHz). This justifies the hypothesis on which the evaluation (11) of the DDM computing time is based, and we may estimate that, for this particular example ($N = 4$ and $L = 10$), TCPU(DDM) < 0.6 TCPU($P_{\rm ABC}$)—we recall that for $\ell = L$, only the problem P_1^L is solved [see (9)], so that $L \simeq 9$ in (11). As an indication, we give on Fig. 12 the values of TCPU(DDM) corresponding to the various calculations. Note that the elementary matrices of A_i are entirely recomputed at each iteration.

V. Conclusions

The DDM proposed in [20] for the solution of 2-D problems has been extended to the 3-D vector case, and the TC's can be implemented in the inhomogeneous domain, thus further reducing the memory storage. It has been demonstrated in [21] that the algorithm converges to the solution of the original problem when zero-order ABC and TC's are employed. The numerical results presented in Section IV show that the same conclusion holds true for second-order conditions, and that the DDM characteristics established for 2-D problems [20] are also valid in 3-D. Because of the large numbers of unknowns each subproblem is solved with a CG, and it has been found to be more advisable, in terms of computing times, to use the zero-order TC, despite the superior efficiency of the second-order one. Thus, the DDM presented in this paper has allowed the solution of a very large problem involving more than $1.3.10^6$ elements and $1.6.10^6$ unknowns with a reasonable number of iterations, while employing the standard edge-based FE formulation. The accuracy achieved with the ABC2 at 800 MHz and 1.2 GHz on the stealth cone sphere with $Z = 1$ or coated with an absorbing material may be considered as satisfactory on a 50-dB dynamic range (the RCS error is lower than 5 dB for a distance d object to boundary equal to 30 cm).

However, the fact that the numerical noise generated by the spurious reflections on the boundary depends, except for low frequencies, on d and not on d/λ implies that a similar accuracy will be obtained at higher frequencies only if a large number of subdomains is implemented, thereby leading to very large computing times, and considerable difficulties in mesh generation especially since the meshes of the interfaces have been constrained here to be identical for adjacent subdomains in order to facilitate the numerical implementation. This constraint could be suppressed if the subdomains are separately meshed and an interpolation scheme is devised that links the unknowns on both sides of an interface. Finally, the substitution of an integral equation to the ABC would allow to achieve a better accuracy with

greater reliability: Considering the infinite free-space domain exterior to the object as an additional subdomain, only the inhomogeneous coating should be meshed, thereby reducing the number of subdomains, and the corresponding DDM algorithm has been shown to converge to the solutions of the exact scattering problem [21].

APPENDIX

Let us assume, for the sake of simplicity, that only the first subdomain Ω_1 does not contain free-space. On account of the continuity of the tangential components of the fields on S_1, the RCS is computed from the following vector quantity:

$$\underline{F}^{\ell}(\underline{u}_r) = -\frac{ik_0}{4\pi}\int_{S_1}[\underline{n}(\underline{r}')\times\underline{H}_1^{\ell}(\underline{r}') + \underline{u}_r\times\underline{n}(\underline{r}')\times\underline{E}_1^{\ell}(\underline{r}')]f(\underline{r}')\,d\underline{r}'$$
$$f(\underline{r}') = e^{ik_0\underline{u}_r\cdot\underline{r}'} \tag{A.1}$$

where $\underline{u}_r$ is the unit vector pointing in the direction of observation. From the third equation in (2a) and the definition (2c) of $T^{\pm}$, the integral on the electric field in (A.1) becomes

$$\frac{ik_0}{4\pi}\int_{S_1}[\underline{n}(\underline{r}')\times\underline{E}_1^{\ell}(\underline{r}')]f(\underline{r}')\,d\underline{r}' = \underline{I}^{\ell}(\underline{u}_r) + \frac{1}{4\pi}\int_{S_1}\left[\underline{\underline{\beta}}+\gamma(L_R+L_D)\right]\underline{H}_{1tg}^{\ell}(\underline{r}')f(\underline{r}')\,d\underline{r}'$$

with

$$\underline{I}^{\ell}(\underline{u}_r) = \frac{1}{4\pi}\int_{S_1} T^{+}\,\underline{H}_1^{\ell}(\underline{r}')f(\underline{r}')\,d\underline{r}'.$$

Then, because of the TC on S_1, $\underline{I}^{\ell}$ can be recursively computed as follows:

$$\underline{I}^{1}(\underline{u}_r) = \frac{1}{4\pi}\int_{S_1} T^{+}\underline{H}^{\mathrm{inc}}(\underline{r}')f(\underline{r}')\,d\underline{r}'$$
$$\ell\geq 2:\ \underline{I}^{\ell}(\underline{u}_r) = \underline{I}^{\ell-1}(\underline{u}_r) + \frac{1-\alpha_\ell}{2\pi}\int_{S_1}\left[\underline{\underline{\beta}}+\gamma(L_R+L_D)\right]\cdot(\underline{H}_{1tg}^{\ell-1}-\underline{H}_{2tg}^{\ell-1})f(\underline{r}')\,d\underline{r}'.$$

REFERENCES

[1] X. Yuan, "Three-dimensional electromagnetic scattering from inhomogeneous objects by the hybrid moment and finite element method," *IEEE Trans. Microwave Theory Tech.*, vol. 38, pp. 1053–1058, 1990.

[2] B. Stupfel, R. Le Martret, P. Bonnemason, and B. Scheurer, "Solution of the scattering problem by axisymmetrical penetrable objects with a mixed boundary-element and finite-element method," in *Proc. Journées Int. Antennes*, Nice, France, Nov. 1990, pp. 116–119.

[3] W. E. Boyse and A. A. Seidl, "A hybrid finite element method for near bodies of revolution," *IEEE Trans. Magn.*, vol. 27, pp. 3833–3836, 1991.

[4] P. Soudais, "Computation of the electromagnetic scattering from complex 3D objects by a hybrid FEM/BEM method," *J. Electromagn. Waves Appl.*, vol. 9, pp. 871–886, 1995.

[5] A. F. Peterson, "Absorbing boundary conditions for the vector wave equation," *Microwave Opt. Tech. Lett.*, vol. 1, pp. 62–64, 1988.

[6] J. Jin, *The Finite Element Methods in Electromagnetics*. New York: Wiley, 1993.

[7] B. Stupfel, "Absorbing boundary conditions on arbitrary boundaries for the scalar and vector wave equations," *IEEE Trans. Antennas Propagat.*, vol. 42, pp. 773–780, 1994.

[8] F. Collino and P. Joly, "New absorbing boundary conditions for the finite element solution of 3-D Maxwell's equations," *IEEE Trans. Magn.*, vol. 31, pp. 1696–1701, 1995.

[9] R. Cicchetti, "A class of exact and higher-order surface boundary conditions for layered structures," *IEEE Trans. Antennas Propagat.*, vol. 44, pp. 249–259, 1996.

[10] B. Stupfel and M. Mognot, "Implementation and derivation of conformal absorbing boundary conditions for the vector wave equation," *J. Electromagn. Waves Appl.*, vol. 12, pp. 1653–1677, 1998.

[11] Z. S. Sacks, D. M. Kingsland, R. Lee, and J. F. Lee, "A perfectly matched anistropic absorber for use as an absorbing boundary condition," *IEEE Trans. Antennas Propagat.*, vol. 43, pp. 1460–1463, 1995.

[12] J. Y. Wu, D. M. Kingsland, J. F. Lee, and R. Lee, "A comparison of anistropic PML to Bérenger's PML and its application to the finite-element method for electromagnetic scattering," *IEEE Trans. Antennas Propagat.*, vol. 45, pp. 40–50, Jan. 1997.

[13] M. Kuzuoglu and R. Mittra, "Investigation of nonplanar perfectly matched absorbers for finite element mesh truncation," *IEEE Trans. Antennas Propagat.*, vol. 45, pp. 474–486, 1997.

[14] F. L. Teixeira and W. C. Chew, "Analytical derivation of a conformal perfectly matched absorber for electromagnetic waves," *Microwave Opt. Tech. Lett.*, vol. 17, pp. 231–236, 1998.

[15] B. Després, Ph.D dissertation, Université Paris IX Dauphine, Paris, France, 1991.

[16] ——, "Domain decomposition method and the Helmholtz problem," in *Proc. Int. Symp. Math. Numer. Aspects Wave Propagat. Phenomena*, 1992, pp. 44–52.

[17] ——, "Domain decomposition method and the Helmholtz problem (part II)," in *Proc. 2nd Int. Conf. Math. Numer. Aspects Wave Propagat.*, 1993, pp. 197–206.

[18] ——, "A domain decomposition method for the harmonic Maxwell equations," in *Iterative Methods in Linear Algebra*, R. Beauwens and P. de Groen, Eds. Amsterdam, The Netherlands: Elsevier, 1992, pp. 475–484.

[19] V. V. Shaidurov and E. I. Ogorodnikov, "Some numerical method of solving Helmholtz equation wave equation," in *Proc. Int. Symp. Math. Numer. Aspects Wave Propagat. Phenomena*, 1992, pp. 73–79.

[20] B. Stupfel, "A fast domain decomposition method for the solution of electromagnetic scattering by large objects," *IEEE Trans. Antennas Propagat.*, vol. 44, pp. 1375–1385, 1996.

[21] B. Stupfel and B. Després, "A domain decomposition method for the solution of large electromagnetic scattering problems," *J. Electromagn. Waves Appl.*, vol. 13, pp. 1553–1568, 1999.

[22] P. Bonnemason and B. Stupfel, "Modeling high frequency scattering by axisymmetric perfectly or imperfectly conducting scatterers," *Electromagn.*, vol. 13, pp. 111–129, 1993.

Bruno Stupfel received the Diplôme d' Ingénieur from the École des Mines de Nancy, France, in 1977, and the Ph.D. degree in solid-state physics from the University of Strasbourg, France, in 1980.

From 1980 to 1982, he was with the Division Tubes Électroniques of Thomson-CSF, where he worked on the development of traveling wave tubes. From 1982 to 1988 he was with the Acoustics Laboratory of the Institut Supérieur d' Électronique du Nord, where he worked on integral equation methods and on the finite-element modeling of hydrophones. in 1988 he joined the Commissariat à l' Énergie Atomique, first at the CEL-V, where he was engaged in the development of computer codes, and since 1996, at the CESTA. During the academic year 1993-1994, he was a Visiting Scholar at the Electromagnetic Communication Laboratory of the University of Illinois at Urbana-Champaign. His research interests include integral equation and finite-element methods in electromagnetics.

Martine Mognot has been with the Commissariat à l' Énergie Atomique since 1981, first at the CEV-M and, since 1996, at the CESTA. She is in charge of the generation of the finite-element meshes that are required for numercal computations in electromagnetics.